CHEMISTRY OF MATERIALS

pubs.acs.org/cm

Article

Molecular Engineering of Atomically Precise Silver Clusters into 2D and 3D Framework Solids

Wakeel Ahmed Dar, Arijit Jana, Korath Shivan Sugi, Ganesan Paramasivam, Mohammad Bodiuzzaman, Esma Khatun, Anirban Som, Ananthu Mahendranath, Amrita Chakraborty, and Thalappil Pradeep*

Cite This: *Chem. Mater.* 2022, 34, 4703−4711

Read Online

ACCESS | Metrics & More | Article Recommendations | Supporting Information

ABSTRACT: Two- and three-dimensional (2D and 3D) atomically precise nanocluster (NC)-based metal−organic frameworks (MOFs) with properties richer than those of NCs themselves are emerging materials. However, fabricating such materials with good stability has not been easy. In this work, a facile synthetic strategy was employed for the creation of silver NC−MOFs starting from $[Ag_{12}(TBT)_7(TFA)_4(CH_3CN)_6]^+$, facilitated by heterocyclic amines, 4,4′-bipyridine (bpy) and pyrazine (pyz), via metal−metal and metal-sulfide rearrangement reactions, where TBT and TFA are tertiarybutylthiolate and trifluoroacetate, respectively. In one of the reactions, the pyz ligand facilitates the formation of a 2D framework with a trigonal crystal system, which exhibits high stability and emits bright green luminescence at low temperatures. Owing to its facile synthesis, good stability, efficient luminescence, uniform porosity, and layered structure, the resultant hexagonal 2D nanosheets can be efficiently exfoliated from parent crystals. The 2D nanosheets are structurally similar to graphene. A top-down approach was employed for the exfoliation of stable 2D nanosheets with lateral dimensions in the range of 0.156 μm. In another case, the bpy ligand induces the construction of a 3D framework with an orthorhombic crystal system. Owing to its interpenetrated AB···AB structure, robustness, and efficient green luminescence at room temperature, the resultant 3D MOF is capable of functioning as a high-performance luminescent sensor for selective detection of explosive analogues, 2-nitrotoluene and 2,4-dinitrotoluene, with excellent recyclability. However, in the absence of the heterocyclic amines, a pristine AgNC was formed. Time-dependent density functional theory calculations were employed to understand the mechanism of energy transfer in AgNC-MOFs. Our strategy offers an unprecedented approach in which heterocyclic amines facilitate intramolecular rearrangement reactions, resulting in 2D and 3D atomically precise NC framework materials. This work not only demonstrates the creation of 2D and 3D materials but also provides new insights into the critical surface coordination chemistry controlled by heterocyclic amines for defining the morphology and properties of cluster frameworks.

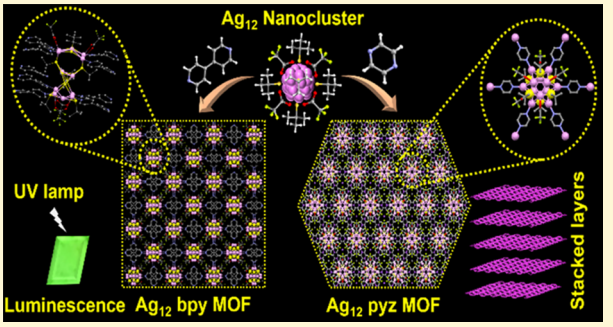

INTRODUCTION

Synthetic methodologies for the design and engineering of atomically precise noble metal nanoclusters (NCs), especially those of gold and silver, have witnessed burgeoning research interest in the past decade because of their architectural diversity and precise tuning of physical properties.[1,2] NCs are stabilized by a variety of surface anchoring ligands such as thiolates,[3−11] imine thiolates,[12] phosphines,[13−15] alkynyls,[16−18] and so forth. The stabilizing ligands are critical not only for maintaining their structures with atomic precision but also for controlling many of their unique properties.[1,7,10,11,19−23] NCs have sizes between discrete atoms and plasmonic nanoparticles. The exceptional properties of NCs, such as their precise nuclearity, quantized electronic energy levels, spectroscopic signatures, intercluster reactions, and so forth, strongly support their molecular behavior.[10] Structural analyses of NCs confirm their precise atomic arrangements, which are indispensable for understanding their properties in great detail.[1,24] Rich structural diversity among NCs was revealed by single-crystal X-ray diffraction (SCXRD).[3,5,7,9,22,25−28] Instability of many of the AgNCs has, however, hindered comprehensive studies including their luminescence and electronic absorption properties since they are susceptible to decomposition even under mild activation. To improve the applicability of AgNCs, organic linkers such as 4,4′-bipyridine (bpy) or 1,2-bis(4-pyridyl)ethane were introduced to connect the adjacent NCs, which resulted in silver NC-based metal−organic frameworks (AgNC-MOFs).[29−32] Investigations of AgNC-MOFs are still at an early stage.[30−37] Constructed from

Received: March 1, 2022
Revised: April 26, 2022
Published: May 11, 2022

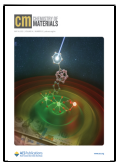

https://doi.org/10.1021/acs.chemmater.2c00647
Chem. Mater. 2022, 34, 4703−4711

the assembly of NCs, AgNC-MOFs represent a novel class of solids with metal-rich nodes, and they demonstrate efficient integration of properties of component NCs as well as linker molecules. Augmentation of rigid structures substantially increases the stability of NC-based frameworks as well as their characteristics, including stability, luminescence, and electronic properties, over pristine NCs.[29] These frameworks have uniform NC nodes, resulting in integrated structures, wide channels, and most significantly, unusual robustness.[29−32] These are favorable for catalysis also.[33] Zang et al. reported the first AgNC-MOF in which the adjacent NCs were coordinated via a bidentate connector, 4,4′-bipyridine.[29] After that, several AgNC-MOFs composed of Ag_8, Ag_{10}, Ag_{12}, Ag_{14}, Ag_{15}, and Ag_{27} have been synthesized with different organic linkers.[30−37] These materials are useful for various applications such as molecular sensors for detecting traces of ethanol in breath,[29] ratiometric sensing of oxygen,[33] sensing of chloromethanes,[31] carbon dioxide fixation,[37] and photocatalytic oxidation of the mustard gas simulant, namely 2-chloroethyl ethyl sulfide.[38] The number of metal atoms in a cluster, its structure, and the type of coordinating ligand modify the properties of the framework system. Understanding synthetic methodologies for the design and engineering of cluster-based frameworks with good stability and efficient luminescence at normal temperature and pressure (NTP) will be useful for designing new materials for specific applications, including explosive detection, energy storage, catalysis, and so forth.

2D materials beyond graphene have attracted intense research interest because of their unexpected physicochemical properties arising from their distinctive 2D morphology, precise thickness, quantum size effect, high electron mobility, and so forth.[39] Compared to the widely studied 2D nanosheets of transition metal dichalcogenides, graphene, hexagonal boron nitride, and others, 2D nanosheets of AgNC-MOFs with unique structural composition are a recent addition to the class of 2D nanomaterials. Thin and homogenous AgNC-MOF nanosheets with more intriguing structures and properties may be useful for prospective applications compared to their bulk counterparts. To create 2D AgNC-MOF nanosheets enriched with NC nodes, a top-down approach may be employed, in which bulk crystals could be delaminated or exfoliated into single layers using a solution-sonication technique. Such a top-down method may be effective in constructing stable AgNC-MOF nanosheets with rational shapes.

With this thought, we have prepared atomically precise 2D nanosheets using delamination or exfoliation of pristine AgNC-MOF crystals. The AgNC-MOF, with the chemical composition $\{[Ag_{12}(TBT)_6(TFA)_6(pyz)_6]\cdot 2CH_3CN\}_n$ (TBT = tertiarybutylthiolate, TFA = trifluoroacetate, and pyz = pyrazine) denoted as (**1**), was synthesized by the reaction of silver thiolate and silver trifluoroacetate with pyrazine, and it showed exceptional stability for more than a year. The pristine MOF crystals were first physically and structurally analyzed and then delaminated or exfoliated using a top-down approach to yield 2D nanosheets. 2D sheets of (**1**) are similar to graphene and associated with metal-rich nodes. We also developed a 3D AgNC-MOF, denoted as (**2**), with a honeycomb-like structure with the chemical formula $\{[Ag_{12}S_2(TBT)_8(TFA)_4(bpy)_8]\cdot bpy\}_n$ (bpy = 4,4′-bipyridine) using a similar reaction procedure, except that instead of pyz, bpy was employed. In addition to their stability, lamellar morphology, and luminescent properties, thin films of this framework with exceptional photostability can serve as efficient luminescent sensors with sensitivity and selectivity for the detection of aromatic nitrotoluenes [2-nitrotoluene (NT) and 2,4-dinitrotoluene (DNT)], surrogates for explosives. Without heterocyclic amines, a pristine $[Ag_{12}(TBT)_7(TFA)_4(CH_3CN)_6]^+$ NC, denoted as Ag_{12}, was obtained. In all the cases, Ag_{12} serves as the basic unit with different geometric arrangements and shows different bonding patterns in both frameworks. From the structural analysis, it is evident that pyz and bpy induce intramolecular metal−metal and metal−sulfide rearrangements in the Ag_{12} NC to yield 2D (**1**) and 3D (**2**) frameworks, respectively. Both of these are different in geometry, structural composition, morphology, and physical properties.

RESULTS AND DISCUSSION

Synthesis and Characterization of AgNC-MOFs. Synthetic approaches for AgNC-MOFs and pristine Ag_{12} NC are schematically presented in Figure 1. In brief, the AgNC-

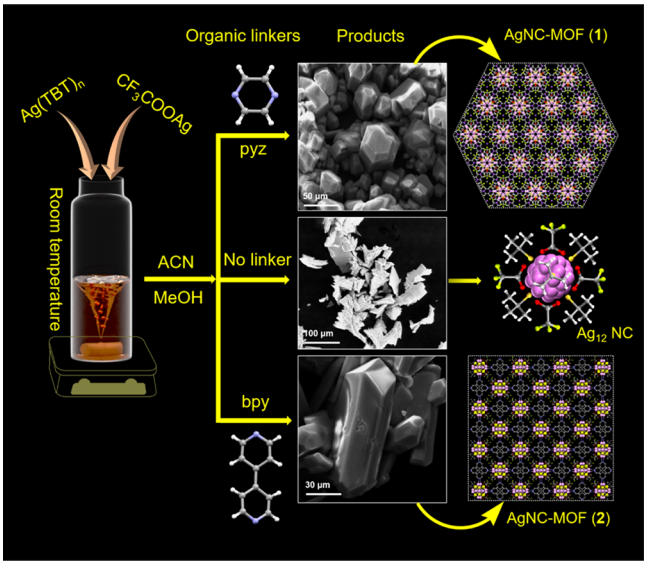

Figure 1. Schematic representation of the synthesis of AgNC-MOFs: (**1**) (top-right) and (**2**) (bottom-right) are crystal structures of the product, and without an organic linker, Ag_{12} NC (middle) was obtained. ACN-acetonitrile; MeOH-methanol. Color codes: Ag light pink; S yellow; C gray; N magenta; F green; H white; and O red.

MOF (**1**) was synthesized by adding an equal amount of silver thiolate and silver trifluoroacetate precursors in a 1:1 solvent mixture of acetonitrile (ACN) and methanol. Subsequently, the pyz ligand was added to the reaction mixture, and stirring was continued for 2 h. The reaction product was filtered and kept for slow evaporation at a low temperature (10 ± 5 °C), and after one week, polyhedral-shaped crystals were obtained (Figure 1). AgNC-MOF (**2**) with rod-shaped crystals was obtained using the same reaction procedure, except that instead of pyz, bpy was used (Figure 1). However, when no heterocyclic amine was used, pristine Ag_{12} NC was obtained, which was characterized by high-resolution electrospray ionization-mass spectrometry (HR ESI-MS) and UV−vis spectroscopy. AgNC-MOFs (**1**) and (**2**) were structurally characterized by SCXRD, and the phase purity of microcrystals was ascertained by powder X-ray diffraction (PXRD). Additional characterization used thermogravimetric analysis (TGA). Electronic properties were studied by UV−vis and

https://doi.org/10.1021/acs.chemmater.2c00647
Chem. Mater. 2022, 34, 4703−4711

fluorescence spectroscopies. Experimental details are presented in the Supporting Information

Structural Anatomy of AgNC-MOF (1). Product (**1**) was obtained in good yield (~60% in terms of Ag). It crystallizes into a trigonal space group, $P\bar{3}m$. The total structure of (**1**) is shown in Figure 2 and all other structural parameters are

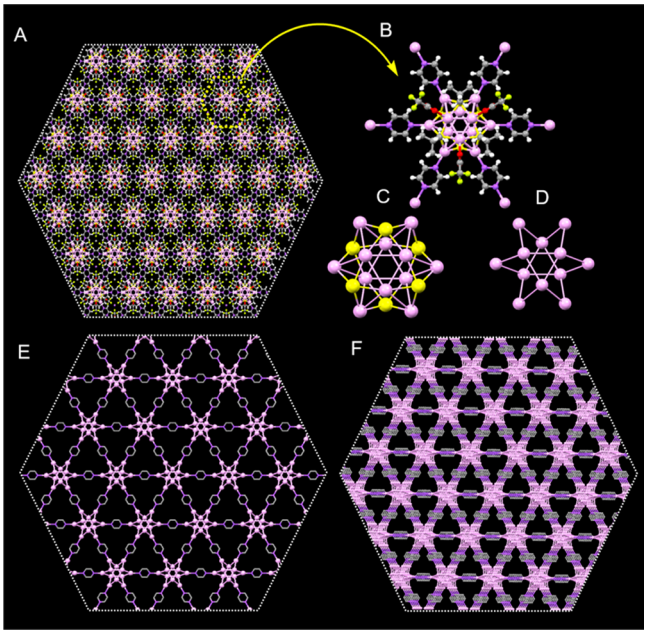

Figure 2. (A) Total crystal structure of (**1**). (B) Structure of the monomeric unit $[Ag_{12}(TBT)_6(TFA)_6(pyz)_6]$. (C) Structure of the hollow cuboctahedron silver-sulfide $Ag_{12}S_6$ core. (D) Structure of the Ag_{12} metallic core without ligands in the *ab*-plane. (E) Structure of (**1**) in the *ab*-plane appears similar to graphene (H atoms as well as *tert*-butyl and TFA groups have been removed for clarity). (F) Layered structure of (**1**). Color codes: Ag light pink; S yellow; C gray; N light blue; F green; and O red.

summarized in Table S1. In the framework structure, metal-rich nodes corresponding to silver chalcogenide ($Ag_{12}S_6$) clusters are interconnected by the bidentate pyz ligand. The geometrical framework holding $Ag_{12}S_6$ at the center can be represented by a sheet connecting 12 Ag and six S atoms, resulting in a hollow cuboctahedron. Considering the arrangement of Ag atoms, the Ag_{12} core can be visualized as three hexagons bisecting each other (Figure S3B). Each $Ag_{12}S_6$ is co-stabilized by six TBT and six TFA ligands. Each TFA ligand is coordinated through one of its O-atoms. Furthermore, each $Ag_{12}S_6$ node is interconnected by six bidentate pyz ligands in a hexagonal planar pattern, forming an infinite 2D framework structure. Rearrangement across the Ag_{12} NC induced by pyz resulted in the formation of (**1**). During the reaction, one TBT unit was eliminated, and two additional TFA units from the reaction mixture were coordinated to the $Ag_{12}S_6$ core to maintain the charge balance. The bond lengths of Ag−Ag, Ag−S, Ag−O, and Ag−N are 3.08, 2.54, 2.39, and 2.33 Å, respectively (Figure S3F). The total structure of this 2D framework in the *ab*-plane is shown in Figures 2A and S4. A cross-section of the framework is shown in Figures 2B and S4C. The structure of the hollow cuboctahedron silver-sulfide $Ag_{12}S_6$ core and Ag_{12} metallic core without ligands is shown in Figure 2C,D. Furthermore, the stacking pattern of the 2D framework layers demonstrates AA···AA parallel packing, with Ag_{12} cluster nodes in neighboring layers completely aligned one above the other (Figure S5). The distance between the adjacent layers considering the nearest Ag atoms of the Ag_{12} core is 7.53 Å. These layers are held together by weak van der Waals interactions and H···F hydrogen bonding between the neighboring layers (average H···F distance of 3.27 Å). ACN molecules occupy voids in the framework structure, which are alternatively positioned above and below the framework pores, with the CH_3 group facing each void (Figure S6). Structural arrangements in different orientations are shown in Figure S7. Along the *bc*-plane, the framework structure of (**1**) shows prominent spacing between the 2D framework layers (Figure S5). It is clear that (**1**) possesses a unique 2D structure, in which NCs joined together by pyz linkers in each layer are similar to graphene (Figures 2E and S4). Figure 2F represents the layered structure of (**1**). The framework structure of this material exhibits enhanced stability for over a year. Therefore, we believe that (**1**) could be an attractive choice for constructing 2D nanosheets.

Micrographs of crystals of (**1**) are shown in Figures 3A−C and S1. The layered structure was visible in them (Figures 3B,C, S1C,D, and S8). It appeared possible to separate these layers. Traditional exfoliating treatments could be effective in terms of efficiency and control over morphology. We, therefore, proceeded with a top-down approach for the scalable fabrication of their nanosheets using the ultrasonication technique. A few crystals were dispersed in 1 mL of ACN in a 2 mL vial, and the mixture was vigorously sonicated for several hours in a 100 W ultrasonic bath, resulting in nanosheets. Figure 3D shows the HR transmission electron microscopy (TEM) image depicting a multilayer AgNC-MOF (**1**) with an interlayer spacing of ~0.72 nm (inset a). In the crystal structure of (**1**), the (010) lattice planes are separated by a distance of 1.13 nm. However, the NC cores from the adjacent layers are separated by 0.75 nm. This distance is seen as the layer with lighter contrast in the TEM image, while NC cores are responsible for a layer with darker contrast (inset a). A slightly smaller distance seen from the TEM image (0.72 nm) is likely due to electron beam-induced structural compaction during image acquisition. A schematic representation of the multilayer structure of AgNC-MOF (**1**) is shown in Figure 3E, in which 2D sheets are stacked one on top of the other through weak interaction and so can be exfoliated easily. High-resolution cryo-TEM micrographs confirm the successful exfoliation of hexagonal 2D nanosheets with lateral dimensions in the micron range (0.156 μm) with structural and morphological features shown in Figures 3D,F,G, S9, and S10. Figure 3H depicts a schematic illustration of a hexagonal cross-section of the total structure in the *ab*-plane, which resembles an exfoliated hexagonal 2D sheet. The creation of 2D nanosheets enriched with metal-rich NC nodes, similar to graphene, opens up a new possibility for the development of 2D functional materials. These findings suggest that the top-down approach is a simple and effective method for the scalable production of NC-based 2D nanosheets, which can be expanded to a wide range of layered cluster-based MOFs. Furthermore, TGA/DTG investigations of crystals of (**1**) under an inert (N_2) atmosphere establish their stability up to 100 °C (Figure S11).

Structural Anatomy of AgNC-MOF (2). SCXRD analysis of (**2**) reveals the formation of a long polymeric or framework structure, namely $\{[Ag_{12}S_2(TBT)_8(TFA)_4(bpy)_8]\cdot bpy\}_n$, which crystallizes in the orthorhombic space group *I*222

https://doi.org/10.1021/acs.chemmater.2c00647
Chem. Mater. 2022, 34, 4703−4711

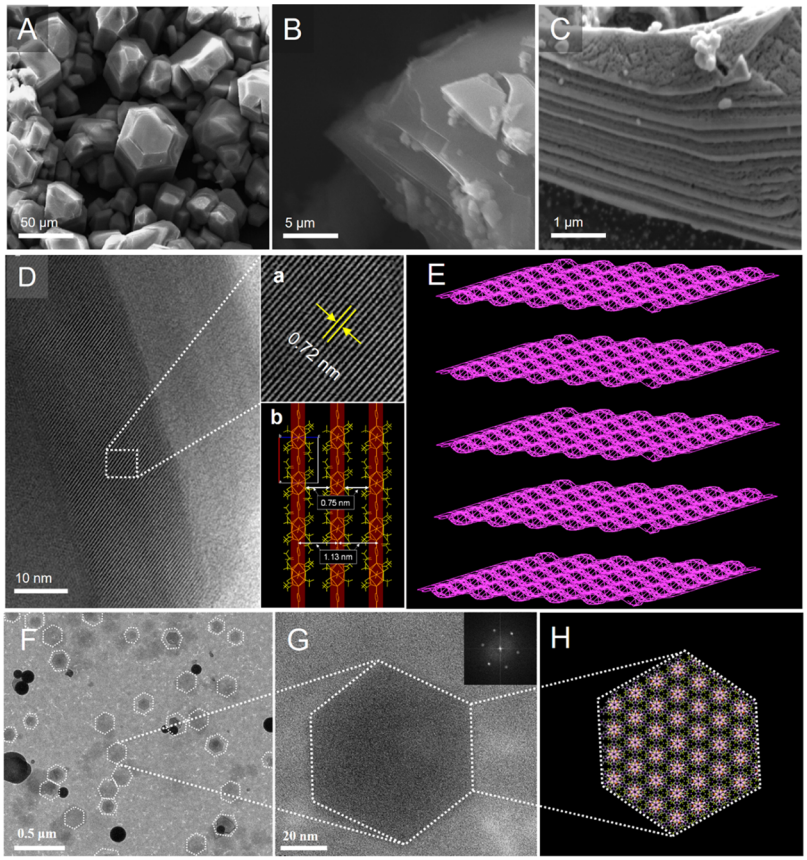

Figure 3. Morphology and structural features of AgNC-MOF (**1**): (A) SEM image of the crystals showing discrete polyhedra. (B,C) FESEM micrographs supporting the layered structure. (D) TEM image showing stacked 2D layers. Inset a: expanded image from the marked area showing an interlayer distance of 0.72 nm. Inset b: schematic showing NCs from adjacent layers separated by a distance of 0.75 nm. The spacing shown is due to the (010) plane of (**1**). (E) Schematic representation of the total crystal structure of (**1**) in which multiple 2D AgNC-MOF sheets are stacked consecutively. (F) HR TEM micrograph showing distinct hexagonal 2D sheets exfoliated from the crystal by sonication. (G) Expanded view of a hexagonal 2D sheet and its electron diffraction pattern (inset). (H) Crystal structure in the *ab*-plane in which the atomic arrangement appears comparable to an exfoliated hexagonal 2D sheet.

(Table S2). The structural details of (**2**) are shown in Figures 4A–D and S12–S16. In the framework structure, all the silver chalcogenide ($Ag_{12}S_{10}$) clusters at the center adopt a dumb-bell-shape, which comprises Ag_5S_4 moieties at the top and bottom and an Ag_2S_2 moiety in the middle (Figure S12). This is an entirely new structure and has not been reported yet. The structural anatomy of Ag_5S_4 and Ag_2S_2 moieties is shown in Figures S12 and S13. Each Ag_{12} cluster node is co-stabilized by eight TBT and four TFA ligands. In addition, each NC node is interconnected by eight bidentate bpy ligands arranged in a square planar bilayer pattern, forming an infinite 3D polymeric honeycomb-like structure, with additional uncoordinated bpy ligands anchored in between the coordinated bpy ligands held together by $\pi-\pi$ interactions (Figures S14 and S15). The bond lengths of Ag–Ag, Ag–S, Ag–O, and Ag–N vary in the range of 2.93–2.97, 2.42–2.55, 2.44–2.57, and 2.35–2.36 Å, respectively (Figure S17). Moreover, these 3D framework layers appear to be interpenetrated with each other, showing an AB···AB packing arrangement. These adjacent 3D layers are held together by F···H interactions between the terminal F-atoms of TFA molecules of one layer and H atoms of bridging bpy units of another layer, which can be best viewed along the *ac*-plane (Figure S15). Thus, a similar rearrangement across the Ag_{12} NC brought about by the bpy ligand resulted in the formation of (**2**). In this case, one additional TBT unit from the solution was added to the NC core to maintain the charge balance. This material is stable for more than a year, and its

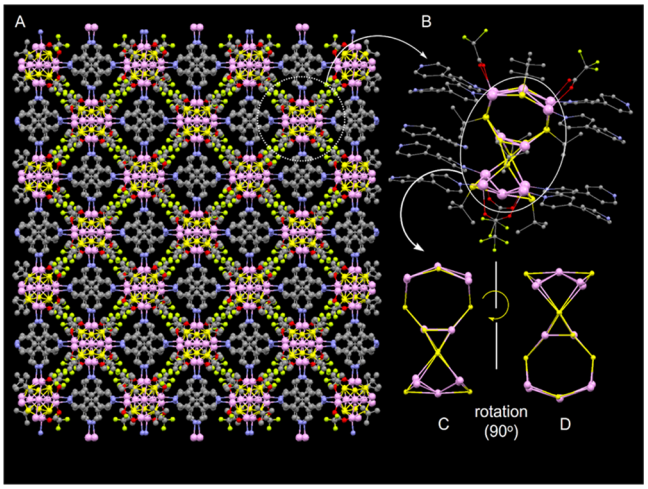

Figure 4. (A) Complete crystal structure of (**2**). (B) Crystal structure of the monomeric unit-$[Ag_{12}S_2(TBT)_8(TFA)_4(bpy)_8]$. (C,D) are inner silver-sulfide cores ($Ag_{12}S_{10}$) without ligands having a C_4 symmetry. Color codes: Ag pink; S yellow; C gray; N magenta; F green; and O red.

https://doi.org/10.1021/acs.chemmater.2c00647
Chem. Mater. 2022, 34, 4703–4711

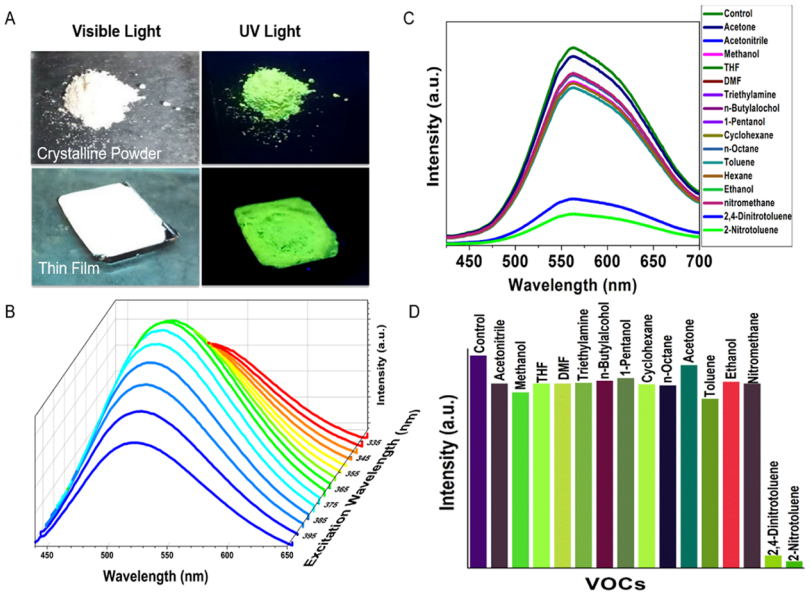

Figure 5. (A) Photograph of the crystalline powder and thin film of (**2**) under visible and UV light. (B) PL spectra of (**2**) crystalline powder at room temperature at various excitations ranging from 330 to 400 nm. (C) PL of thin films of (**2**) independently exposed to the vapors of various organic molecules, excited at 370 nm. (D) Bar graph showing the sensitivity of thin films of (**2**) exposed to the vapors of various organic solvents.

properties are insensitive to air/O_2. From thermograms (Figure S18), it was observed that material (**2**) was thermally stable up to 145 °C. The phase purity of (**1**) and (**2**) was ascertained by PXRD (Figures S19 and S20). We attempted to separate the adjacent layers from each other in (**2**); however, we were unable to obtain the component layers, unlike in (**1**). This could be due to the strong $\pi-\pi$ stacking interactions between the bpy ligands and strong hydrogen bonding (H···F ∼ 2.49 Å) interactions between F-atoms of the CF_3 group and H atoms of the bpy ligand of adjacent layers in (**2**).

Understanding the Ag_{12} NC. Ag_{12} NC was obtained by a reaction between silver thiolate and silver trifluoroacetate in a solvent mixture of methanol and ACN without the use of any organic connectors (bpy and pyz). The obtained reaction product was initially analyzed by UV−vis spectroscopy and HR ESI-MS (Figures S21 and S22). The ESI-MS spectrum (shown in Figure S22) shows a peak at m/z 2616, and it matches well with the molecular composition of $[Ag_{12}(TBT)_7(TFA)_4(CH_3CN)_6]^+$. To identify the counter ion, the IR (infrared) spectrum of a few crystals of Ag_{12} NC was recorded. The IR spectrum revealed a distinct band at 1364 cm^{-1} attributed to the N−O stretching of NO_3^-, indicating it to be the counter ion in this case. NO_3^- has its origin from $AgNO_3$ used during the synthesis of $Ag(TBT)_n$. The product solution was kept for crystallization at room temperature; and after a few days, the crystalline product was obtained. The resulting crystals were unstable and showed no X-ray diffraction. The UV−vis spectrum and HR ESI-MS of this sample solution match well with those reported for Ag_{12} NC.[26] We, therefore, suggest that the addition of organic connectors, that is, bpy or pyz, causes a major structural change in the NC system via intramolecular metal−metal and metal−sulfide rearrangements, which leads to the formation of stable 3D and 2D AgNC-MOFs. This suggests that organic connectors actively promote intramolecular rearrangement in Ag_{12} NC. To the best of our knowledge, this is the first example of an intramolecular metal−metal and metal−sulfide rearrangement reaction in AgNCs promoted by heterocyclic amines.

Photoluminescence. A variety of AgNCs have been reported so far. However, they show less stability and poor luminescence at room temperature. The structural modifications of AgNCs and their transformation into AgNC-MOFs using suitable organic connectors circumvent this problem.[29−31] The AgNC-MOFs (**1**) and (**2**) reported in this work exhibit enhanced stability and efficient photoluminescence (PL).

PL of AgNC-MOF (2). Freshly prepared crystals of (**2**) emit bright green luminescence upon UV light exposure at NTP (Figures 5A and S23). To our delight, this material does not show any sensitivity towards oxygen/air, moisture, or fluctuations in room temperature, in contrast to the previously reported framework structures.[29] The spectral profiles of this crystalline material show a single broad emission band in the green region recorded at various excitations shown in Figure 5B. The excitation at 370 nm favors high-energy green emission with a peak maximum at 520 nm. The emission maximum (λ_{em}) changes with a change in the excitation wavelength (Figure S23D). The material remains stable for more than a year, and the structure and PL remain unaffected upon repeated exposure to air/O_2 or temperature fluctuations, ensuring the endurance and robustness of this material. The structure and geometry of Ag_{12} NC nodes are entirely new in this framework structure. The occurrence of efficient PL from (**2**) could be attributed to the perfect alignment of bpy chromophores around atomically precise NCs as well as the framework's rigid structure. This efficiently prevents nonradiative energy loss by inhibiting vibronic coupling in the framework structure.[29] Density functional theory (DFT) calculations reveal that the emission from the excited states of this system arises due to ligand (bpy)-to-metal charge transfer (LMCT) transitions (discussed below). In this case, the fluorescence lifetime in microseconds ($\tau_{em,NTP}$ = 0.138 μs) implies that emission originates from triple excited states.[29] The PL lifetime measurements were calculated upon excitation

https://doi.org/10.1021/acs.chemmater.2c00647
Chem. Mater. 2022, 34, 4703−4711

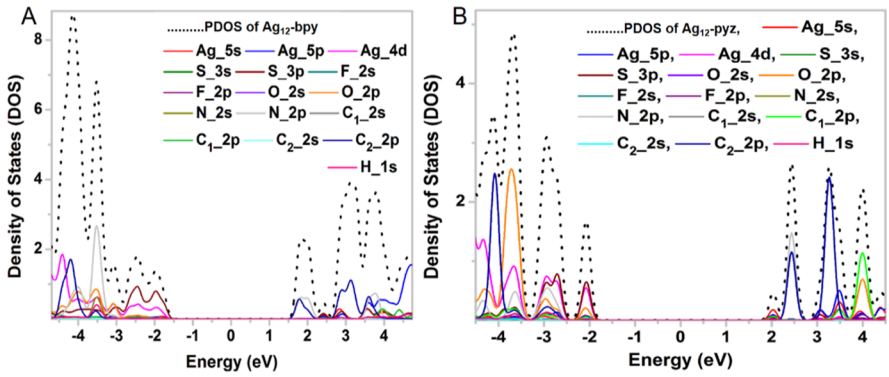

Figure 6. PDOS of (A) Ag_{12}-bpy and (B) Ag_{12}-pyz.

at 370 nm and the emission of 520 nm using a pulse-diode LED as an excitation source (Figure S24). In addition, we investigated the thin films of the same materials for PL studies. Thin films were prepared using the solution drop-casting method (details are presented in the Supporting Information). PL observed from a thin film of (**2**) was almost similar to that of its crystalline powder and was investigated for sensing properties (section on sensing of nitroaromatics) (Figures 5C and S23C). The origin of emission transitions is discussed in detail using DFT calculations (see below).

Understanding of the Electronic Structure of AgNC-MOF (2). Electronic energy levels and transitions of both the MOFs were calculated using time-dependent density functional theory (TD-DFT). To reduce computational complexity, monomeric units, namely $[Ag_{12}(S_2)(TBT)_8(TFA)_4(bpy)_{10}]$ abbreviated as Ag_{12}-bpy, were used in this work. The optimized geometry of this system and the calculated emission spectrum are shown in Figure S25A,B. The total density of states (TDOS) and partial density of states (PDOS) were calculated for the Ag_{12}-bpy unit, and the spectra are plotted in Figure S25C,D. The middle of the highest occupied molecular orbital−lowest unoccupied molecular orbital (HOMO−LUMO) gap was set to zero to correlate with the Fermi level. For the Ag_{12}-bpy system, the contribution of 2p atomic orbitals (AOs) of C atoms has been extensively investigated in the PDOS spectra by separately grouping aliphatic Cs of TBT as C_1 and aromatic carbons of bpy as C_2, as shown in Figure 6A. From the PDOS spectra, we see that the major contribution emerges from the 2p (π orbitals, C_2) AOs of bpy ligands along with 2p AOs of N atoms. This indicates that the π−orbitals of bpy ligands play a substantial role in the emission transitions that emerge from the lowest LUMOs of the cluster system. Therefore, we believe that ligand (bpy)-to-metal charge transfer (LMCT) is primarily responsible for the emission transitions in the Ag12-bpy system.

PL of AgNC-MOF (1). The crystals of (**1**) under UV light do not show any detectable luminescence at room temperature; however, a bright green luminescence was observed at low temperatures (shown in Figure S27). The solid-state PL spectrum recorded under 365 nm excitation displays a brilliant green emission band with a peak maximum at 510 nm at a low temperature (80 K) (Figure S27). The optimized geometry of the monomeric unit, namely $[Ag_{12}(TBT)_6(TFA)_6(pyz)_6]$ denoted as Ag_{12}-pyz is shown in Figure S28A. TDOS and PDOS spectra of Ag_{12}-pyz are plotted in Figures 6B and S28C,D. In the PDOS spectra, the contributions of 2p AOs of C atoms were investigated in detail by separately grouping them into aliphatic (TBT) and aromatic (pyz) carbons, denoted as C_1 and C_2, respectively. The PDOS spectra show that the contribution of 2p (π orbitals, C_2) AOs of pyz ligands, as well as 2p AOs of nitrogen atoms, are shifted away from the LUMOs and are likely to be dominant at 3.1 eV, thereby minimizing their dominance in higher unoccupied MOs. This suggests that π−orbitals of the pyz ligand are not involved in emission transitions. Therefore, the emission from the Ag_{12}-pyz system could be attributed to the metal-to-ligand charge transfer.

UV−Vis Absorption Spectroscopy. UV−vis absorption measurements were carried out for all the reaction products, namely Ag_{12} NC and AgNC-MOFs (**1**) and (**2**) as ACN solutions. The absorption spectrum of Ag_{12} NC was similar to that reported previously (Figure S21).[26] The UV−vis absorption spectrum of (**1**) and pristine pyz are nearly identical and display a broad absorption band in the window of 215−340 nm with a maximum at λ_{max} 260 nm, followed by shoulder peaks (Figure S30). These peaks can be assigned to $\pi-\pi^*$ and $n-\pi^*$ (C═C and C═N) transitions of the pyz ligand. The calculated absorption spectrum of Ag_{12}-pyz displays a broad absorption band between 209 and 355 nm. UV−vis spectra of (**2**) and the free bpy ligand show nearly identical absorption bands with maxima (λ_{max}) at 237 nm (Figure S31). These peaks could be due to the $\pi-\pi^*$ and $n-\pi^*$ (C═C and C═N) transitions of the bpy ligand present in the system. The calculated spectrum displays a broad absorption band in the region between 220 and 450 nm with one intense peak at 234 nm followed by small shoulder peaks at 260 and 285 nm. The optimized structure of the Ag_{12}-bpy system suggests that absorption peaks in (**2**) emerge from bpy ligands only. Therefore, all absorption transitions appearing in both the frameworks could be attributed to $\pi-\pi^*$ and $n-\pi^*$ transitions of C═C and C═N of linkers.

Photostability of AgNC-MOF (2). One of the major challenges for silver-based NCs is their sensitivity towards light, which restricts their use as photocatalysts. The interaction of silver-based NCs with photons generates electrons easily, allowing Ag^+ to be quickly converted to metallic Ag. As a result, obtaining photostable Ag-based NCs for photocatalytic activities remains a challenge. Thin films of (**2**) were exposed to UV and visible light to investigate their photostability. The integrated emission intensity (λ_{em} 520 nm) was monitored separately under uninterrupted exposure of 370 and 500 nm radiations in the UV and visible regions, respectively, for 2000 s (Figure S32). Results show that

https://doi.org/10.1021/acs.chemmater.2c00647
Chem. Mater. 2022, 34, 4703−4711

degradation has been greatly reduced compared to pristine Ag_{12} NCs. The photostability of framework materials could be attributed to their rigid double-layer structure and the shielding of silver atoms by organic ligands. This could make them promising candidates for photocatalysis.

Sensing of Nitroaromatics. PL from thin films of (**2**) was studied for fluorescence sensing. Prior to exposure, thin films were first activated by passing dry air to remove traces of trapped solvents. In all cases, the PL spectra of thin films of (**2**) were recorded at λ_{ex} 370 nm. The emission spectrum of a pristine thin film of (**2**) is shown in Figure 5C. The thin films were then exposed separately to various organic solvent vapors such as ACN (1), methanol (2), ethanol (3), tetrahydrofuran (4), DMF (5), triethylamine (6), *n*-butyl alcohol (7), 1-pentanol (8), cyclohexane (9), *n*-octane (10), acetone (11), toluene (12), nitromethane (13), NT (14), and DNT (15). Just after their exposure, PL was recorded (shown in Figure 5C,D). The emission intensity changed drastically upon exposure to NT and DNT vapors. Other solvents (1−13) did not induce any significant variation in the luminescence intensity of the thin films. This suggests the higher sensitivity of (**2**) towards NT and DNT. To demonstrate the sensitivity, thin films of (**2**) were exposed to the equilibrated vapors of NT (ca. 200 ppm at 25 °C) and DNT (ca. 0.0018 ppm at 25 °C) for different time intervals such as 15, 30, 50, 100, 150, and 200 s. After 15 s of analyte exposure, the emission intensities of thin films were drastically reduced by NT and DNT (Figure 5C,D). Exposure of thin films to analyte vapors beyond 30 s resulted in no further quenching, and the response time of (**2**) for each analyte appears to be 15 s. We measured the time-dependent fluorescence quenching for NT and DNT. The percentage quenching efficiencies $[((I_o - I)/I_o) \times 100$; I_o being the luminescence intensity of the pristine thin film, while I is the luminescence intensity after exposure to a selected analyte] of thin films of (**2**) upon exposure to the equilibrated vapors of NT and DNT at different time intervals are shown in Figure S33. The percentage quenching efficiencies of NT and DNT are 84 and 74%, respectively. The higher quenching efficiency of NT is likely due to its higher vapor pressure.[40] After being exposed to NT and DNT, thin films of (**2**) were kept in an oven at 45 °C for 20 min, and the emission was regained. The process could be repeated several times without any loss of efficiency, which establishes the reusability of the material. The quenching of PL could be due to the transfer of energy from the HOMOs of the excited (**2**) to the LUMOs of nitro-aromatic compounds (NT and DNT), which are strong π−acceptors (Figure S35).[41] When exposed to the vapors of aliphatic nitro compounds, the emission intensity does not show a considerable change. These findings suggest that this material can distinguish between aliphatic and aromatic nitro compounds and can serve as an efficient fluorescent sensor for the detection of explosives.

CONCLUSIONS

In summary, a heterocyclic amine-assisted rearrangement approach can be adapted to construct 2D and 3D silver cluster-based metal−organic frameworks. The pyz and bpy organic connectors facilitate the construction of 2D $\{[Ag_{12}(TBT)_6(TFA)_6(pyz)_6]\cdot 2CH_3CN\}_n$ (**1**) and 3D $\{[Ag_{12}S_2(TBT)_8(TFA)_4(bpy)_8]\cdot bpy\}_n$ (**2**) frameworks, respectively, under similar reaction conditions. Each framework material exhibits different morphology, structure, and physical properties. The synthesized atomically precise NC-based 2D framework material promoted by pyz is associated with its distinguishing characteristics such as a simple synthetic method, good yield, enhanced stability, uniform porosity, metal-rich nodes, brilliant luminescence, and a layered structure. Ultrasonication-assisted top-down exfoliation of the parent crystals of (**1**) results in nanosheets, and each layer appears structurally similar to graphene. Creating 2D nanosheets in the exotic class of atomically precise materials with metal-rich NC nodes and effectively separating those sheets could open up a new domain in the field of NC chemistry. The bpy ligand-induced 3D framework material has a unique interpenetrated AB···AB packing structure, robustness, good photostability, and displays efficient green luminescence at room temperature. The resulting 3D MOF (**2**) can function as a high-performance luminescence sensor for the selective recognition of explosives such as NT and DNT with recyclability. In the absence of the heterocyclic amine, a pristine $[Ag_{12}(TBT)_7(TFA)_4(CH_3CN)_6]^+$ NC was obtained. Overall, this study presents an efficient synthetic approach for creating 2D and 3D AgNC-MOFs with rich architectural diversity, high-density metallic nodes, and concomitant properties, paving the way for making 2D and 3D framework structures of NCs for advanced applications.

EXPERIMENTAL SECTION

Chemicals. Tertiarybutylthiol (TBT), silver trifluoroacetate (TFA), and silver nitrate ($AgNO_3$) were purchased from Aldrich. All chemicals were used as received without further purification. All the solvents were purchased from Rankem chemicals and were of analytical grade. Silver thiolate $[Ag(TBT)_n]$ used during the reaction was synthesized using the standard procedure.

Synthesis of Silver Cluster-Based Metal−Organic Frameworks and Silver NC. *Synthesis of* $\{[Ag_{12}(TBT)_6(TFA)_6(pyz)_6]\cdot 2CH_3CN\}_n$ *(**1**) MOF.* The AgNC-MOF (**1**) was synthesized by adding 20 mg each of silver thiolate, $Ag(TBT)_n$, and silver trifluoroacetate to a mixture of 2 mL each of ACN and methanol solution. To this was added 20 mg of pyz, and the reaction mixture was kept stirring for 2 h and subsequently filtered. The reaction mixture was kept for slow evaporation at a low temperature (10 ± 5 °C), and after one week, polyhedron-shaped crystals suitable for SCXRD were obtained. The analysis of SCXRD shows the formation of synthesis of $\{[Ag_{12}(TBT)_6(TFA)_6(pyz)_6]\cdot 2CH_3CN\}_n$ (**1**).

Synthesis of $\{[Ag_{12}S_2(TBT)_8(TFA)_4(bpy)_8]\cdot bpy\}_n$ *(**2**) MOF.* AgNC-MOF (**2**) was synthesized following a similar approach to that described above but with a different organic linker, such as bpy. AgNC-MOF (**2**) was synthesized by adding 20 mg each of silver thiolate, $Ag(TBT)_n$, and silver trifluoroacetate to a mixture of 2 mL each of ACN and methanol solution. To this was added 20 mg of bpy, and the reaction mixture was kept stirring for 2 h and subsequently filtered. The filtrate was kept for slow evaporation at a low temperature (10 ± 5 °C) and after one week, rod-shaped crystals suitable for SCXRD were obtained. The analysis of SCXRD shows the formation of synthesis of $\{[Ag_{12}S_2(TBT)_8(TFA)_4(bpy)_8]\cdot bpy\}_n$ (**2**).

Synthesis of $[Ag_{12}(TBT)_7(TFA)_4(CH_3CN)_6]^+$ *NC.* 20 mg each of silver thiolate $[Ag(TBT)_n]$ and silver trifluoroacetate were added to a solution of ACN and methanol (2 mL each). The reaction mixture was kept on stirring for 1 h, and after that, the reaction mixture was left for crystallization at a low temperature. In this method, no organic connector was employed. After a few days, a crystalline powder was obtained that was investigated by UV−vis and ESI-MS measurements, which showed the formation of the $[Ag_{12}(TBT)_7(TFA)_4(CH_3CN)_6]^+$ NC, denoted as Ag_{12}.

Cryo-TEM Sample Preparation. Samples used for TEM analysis were prepared by drop-casting from the ACN dispersions of the samples onto ultrathin (<10 nm thickness) carbon-coated copper grids. The grids were plasma cleaned on a Gatan Solarus (model 950) plasma cleaner for 30 s prior to the sample preparation. TEM images

https://doi.org/10.1021/acs.chemmater.2c00647
Chem. Mater. 2022, 34, 4703−4711

were collected in a low-dose mode on a JEM-3200FSC field-emission cryo-electron microscope (JEOL Ltd.) with an Omega-type zero-loss energy filter operated at 300 kV. The images were acquired with Gatan DigitalMicrograph software, maintaining the specimen temperature at −187 °C to minimize beam-induced damage.

Thin-Film Preparation. Quartz (or glass) slides with a dimension of 16 mm × 16 mm were rinsed with acetone and kept in an oven for 1 h at 80 °C to remove any traces of impurities. Thin films were prepared using a drop-casting method at room temperature. For this, a solution containing (**2**) was filtered to obtain a clear solution. A few droplets of this transparent solution were slowly dropped at the four vertices of the slide until the solution was spread to cover the entire slide. These were left for air drying to obtain a thin coating of AgNC-MOF, which was used to detect nitroaromatics.

■ ASSOCIATED CONTENT

Supporting Information

The Supporting Information is available free of charge at https://pubs.acs.org/doi/10.1021/acs.chemmater.2c00647.

Instrumentation, X-ray crystallographic parameters, HR TEM micrographs, general instrumental parameters used for ESI-MS measurements, additional experimental data, computational details, band gap calculations, and other details (PDF)

Crystallographic data for $\{[Ag_{12}(TBT)_6(TFA)_6(pyz)_6]\cdot 2CH_3CN\}_n$ (**1**) (CIF)

Crystallographic data for $\{[Ag_{12}S_2(TBT)_8(TFA)_4(bpy)_8]\cdot bpy\}_n$ (**2**) (CIF)

■ AUTHOR INFORMATION

Corresponding Author

Thalappil Pradeep − *Department of Chemistry, DST Unit of Nanoscience and Thematic Unit of Excellence, Indian Institute of Technology Madras, Chennai 600036, India;* orcid.org/0000-0003-3174-534X; Email: pradeep@iitm.ac.in

Authors

Wakeel Ahmed Dar − *Department of Chemistry, DST Unit of Nanoscience and Thematic Unit of Excellence, Indian Institute of Technology Madras, Chennai 600036, India*

Arijit Jana − *Department of Chemistry, DST Unit of Nanoscience and Thematic Unit of Excellence, Indian Institute of Technology Madras, Chennai 600036, India*

Korath Shivan Sugi − *Department of Chemistry, DST Unit of Nanoscience and Thematic Unit of Excellence, Indian Institute of Technology Madras, Chennai 600036, India*

Ganesan Paramasivam − *Department of Chemistry, DST Unit of Nanoscience and Thematic Unit of Excellence, Indian Institute of Technology Madras, Chennai 600036, India*

Mohammad Bodiuzzaman − *Department of Chemistry, DST Unit of Nanoscience and Thematic Unit of Excellence, Indian Institute of Technology Madras, Chennai 600036, India*

Esma Khatun − *Department of Chemistry, DST Unit of Nanoscience and Thematic Unit of Excellence, Indian Institute of Technology Madras, Chennai 600036, India*

Anirban Som − *Department of Chemistry, DST Unit of Nanoscience and Thematic Unit of Excellence, Indian Institute of Technology Madras, Chennai 600036, India;* orcid.org/0000-0002-6646-679X

Ananthu Mahendranath − *Department of Chemistry, DST Unit of Nanoscience and Thematic Unit of Excellence, Indian Institute of Technology Madras, Chennai 600036, India*

Amrita Chakraborty − *Department of Chemistry, DST Unit of Nanoscience and Thematic Unit of Excellence, Indian Institute of Technology Madras, Chennai 600036, India*

Complete contact information is available at: https://pubs.acs.org/10.1021/acs.chemmater.2c00647

Notes

The authors declare no competing financial interest.

■ ACKNOWLEDGMENTS

We thank the Department of Science and Technology for supporting our research program. We thank the Sophisticated Analytical Instruments Facility, Indian Institute of Technology, Madras, for SCXRD data collection.

■ REFERENCES

(1) Chakraborty, I.; Pradeep, T. Atomically Precise Clusters of Noble Metals: Emerging Link between Atoms and Nanoparticles. *Chem. Rev.* **2017**, *117*, 8208−8271.

(2) Jin, R.; Zeng, C.; Zhou, M.; Chen, Y. Atomically Precise Colloidal Metal Nanoclusters and Nanoparticles: Fundamentals and Opportunities. *Chem. Rev.* **2016**, *116*, 10346−10413.

(3) Joshi, C. P.; Bootharaju, M. S.; Alhilaly, M. J.; Bakr, O. M. $[Ag_{25}(SR)_{18}]^-$: The "Golden" Silver Nanoparticle. *J. Am. Chem. Soc.* **2015**, *137*, 11578−11581.

(4) Yang, H.; Wang, Y.; Huang, H.; Gell, L.; Lehtovaara, L.; Malola, S.; Häkkinen, H.; Zheng, N. All-Thiol-Stabilized Ag_{44} and $Au_{12}Ag_{32}$ Nanoparticles with Single-Crystal Structures. *Nat. Commun.* **2013**, *4*, 2422.

(5) Khatun, E.; Bodiuzzaman, M.; Sugi, K. S.; Chakraborty, P.; Paramasivam, G.; Dar, W. A.; Ahuja, T.; Antharjanam, S.; Pradeep, T. Confining an Ag_{10} Core in an Ag_{12} Shell: A Four-Electron Superatom with Enhanced Photoluminescence upon Crystallization. *ACS Nano* **2019**, *13*, 5753−5759.

(6) Liu, J.-W.; Feng, L.; Su, H.-F.; Wang, Z.; Zhao, Q.-Q.; Wang, X.-P.; Tung, C.-H.; Sun, D.; Zheng, L.-S. Anisotropic Assembly of Ag_{52} and Ag_{76} Nanoclusters. *J. Am. Chem. Soc.* **2018**, *140*, 1600−1603.

(7) Fenske, D.; Anson, C. E.; Eichhöfer, A.; Fuhr, O.; Ingendoh, A.; Persau, C.; Richert, C. Syntheses and Crystal Structures of $[Ag_{123}S_{35}(S^tBu)_{50}]$ and $[Ag_{344}S_{124}(S^tBu)_{96}]$. *Angew. Chem., Int. Ed.* **2005**, *44*, 5242−5246.

(8) Dass, A.; Theivendran, S.; Nimmala, P. R.; Kumara, C.; Jupally, V. R.; Fortunelli, A.; Sementa, L.; Barcaro, G.; Zuo, X.; Noll, B. C. $Au_{133}(SPh\text{-}TBu)_{52}$ Nanomolecules: X-Ray Crystallography, Optical, Electrochemical, and Theoretical Analysis. *J. Am. Chem. Soc.* **2015**, *137*, 4610−4613.

(9) Harkness, K. M.; Tang, Y.; Dass, A.; Pan, J.; Kothalawala, N.; Reddy, V. J.; Cliffel, D. E.; Demeler, B.; Stellacci, F.; Bakr, O. M.; McLean, J. A. $Ag_{44}(SR)_{304}^{-}$: A Silver-Thiolate Superatom Complex. *Nanoscale* **2012**, *4*, 4269−4274.

(10) Du, Y.; Sheng, H.; Astruc, D.; Zhu, M. Atomically Precise Noble Metal Nanoclusters as Efficient Catalysts: A Bridge between Structure and Properties. *Chem. Rev.* **2020**, *120*, 526−622.

(11) Negishi, Y.; Arai, R.; Niihori, Y.; Tsukuda, T. Isolation and structural characterization of magic silver clusters protected by 4-(tert-butyl)benzyl mercaptan. *Chem. Commun.* **2011**, *47*, 5693−5695.

(12) Jana, A.; Chakraborty, P.; Dar, W. A.; Chandra, S.; Khatun, E.; Kannan, M. P.; Ras, R. H. A.; Pradeep, T. Dual Emitting Ag35nanocluster Protected by 2-Pyrene Imine Thiol. *Chem. Commun.* **2020**, *56*, 12550−12553.

(13) Zhang, Q.-F.; Williard, P. G.; Wang, L.-S. Polymorphism of Phosphine-Protected Gold Nanoclusters: Synthesis and Characterization of a New 22-Gold-Atom Cluster. *Small* **2016**, *12*, 2518−2525.

(14) Sharma, S.; Chakrahari, K. K.; Saillard, J.-Y.; Liu, C. W. Structurally Precise Dichalcogenolate-Protected Copper and Silver Superatomic Nanoclusters and Their Alloys. *Acc. Chem. Res.* **2018**, *51*, 2475−2483.

(15) Sugiuchi, M.; Shichibu, Y.; Konishi, K. An Inherently Chiral Au24 Framework with Double-Helical Hexagold Strands. *Angew. Chem., Int. Ed.* **2018**, *57*, 7855−7859.
(16) Wan, X.-K.; Guan, Z.-J.; Wang, Q.-M. Homoleptic Alkynyl-Protected Gold Nanoclusters: $Au_{44}(PhC{\equiv}C)_{28}$ and $Au_{36}(PhC{\equiv}C)_{24}$. *Angew. Chem., Int. Ed.* **2017**, *56*, 11494−11497.
(17) Lei, Z.; Li, J. J.; Wan, X. K.; Zhang, W. H.; Wang, Q. M. Isolation and Total Structure Determination of an All-Alkynyl-Protected Gold Nanocluster Au_{144}. *Angew. Chem., Int. Ed.* **2018**, *57*, 8639−8643.
(18) Lei, Z.; Wan, X.-K.; Yuan, S.-F.; Guan, Z.-J.; Wang, Q.-M. Alkynyl Approach toward the Protection of Metal Nanoclusters. *Acc. Chem. Res.* **2018**, *51*, 2465−2474.
(19) Fenske, D.; Persau, C.; Dehnen, S.; Anson, C. E. Syntheses and Crystal Structures of the Ag-S Cluster Compounds $[Ag_{70}S_{20}(SPh)_{28}(Dppm)_{10}](CF_3CO_2)_2$ and $[Ag_{262}S_{100}(S^tBu)_{62}(Dppb)_6]$. *Angew. Chem., Int. Ed.* **2004**, *43*, 305−309.
(20) Liu, X.; Chen, J.; Yuan, J.; Li, Y.; Li, J.; Zhou, S.; Yao, C.; Liao, L.; Zhuang, S.; Zhao, Y.; Deng, H.; Yang, J.; Wu, Z. A Silver Nanocluster Containing Interstitial Sulfur and Unprecedented Chemical Bonds. *Angew. Chem.* **2018**, *130*, 11443−11447.
(21) Liu, J. W.; Wang, Z.; Chai, Y. M.; Kurmoo, M.; Zhao, Q. Q.; Wang, X. P.; Tung, C. H.; Sun, D. Core Modulation of 70-Nuclei Core-Shell Silver Nanoclusters. *Angew. Chem., Int. Ed.* **2019**, *58*, 6276−6279.
(22) Li, B.; Huang, R.-W.; Qin, J.-H.; Zang, S.-Q.; Gao, G.-G.; Hou, H.-W.; Mak, T. C. W. Thermochromic Luminescent Nest-Like Silver Thiolate Cluster. *Chem.—Eur. J.* **2014**, *20*, 12416−12420.
(23) Díez, I.; Pusa, M.; Kulmala, S.; Jiang, H.; Walther, A.; Goldmann, A. S.; Müller, A. H. E.; Ikkala, O.; Ras, R. H. A. Color Tunability and Electrochemiluminescence of Silver Nanoclusters. *Angew. Chem., Int. Ed.* **2009**, *48*, 2122−2125.
(24) Yu, H.; Rao, B.; Jiang, W.; Yang, S.; Zhu, M. The Photoluminescent Metal Nanoclusters with Atomic Precision. *Coord. Chem. Rev.* **2019**, *378*, 595−617.
(25) Wang, Z.-Y.; Wang, M.-Q.; Li, Y.-L.; Luo, P.; Jia, T.-T.; Huang, R.-W.; Zang, S.-Q.; Mak, T. C. W. Atomically Precise Site-Specific Tailoring and Directional Assembly of Superatomic Silver Nanoclusters. *J. Am. Chem. Soc.* **2018**, *140*, 1069−1076.
(26) Dar, W. A.; Bodiuzzaman, M.; Ghosh, D.; Paramasivam, G.; Khatun, E.; Sugi, K. S.; Pradeep, T. Interparticle Reactions between Silver Nanoclusters Leading to Product Cocrystals by Selective Cocrystallization. *ACS Nano* **2019**, *13*, 13365−13373.
(27) Bodiuzzaman, M.; Ghosh, A.; Sugi, K. S.; Nag, A.; Khatun, E.; Varghese, B.; Paramasivam, G.; Antharjanam, S.; Natarajan, G.; Pradeep, T. Camouflaging Structural Diversity: Co-Crystallization of Two Different Nanoparticles Having Different Cores But the Same Shell. *Angew. Chem., Int. Ed.* **2019**, *58*, 189−194.
(28) Bi, Y.; Wang, Z.; Liu, T.; Sun, D.; Godbert, N.; Li, H.; Hao, J.; Xin, X. Supramolecular Chirality from Hierarchical Self-Assembly of Atomically Precise Silver Nanoclusters Induced by Secondary Metal Coordination. *ACS Nano* **2021**, *15*, 15910−15919.
(29) Huang, R.-W.; Wei, Y.-S.; Dong, X.-Y.; Wu, X.-H.; Du, C.-X.; Zang, S.-Q.; Mak, T. C. W. Hypersensitive Dual-Function Luminescence Switching of a Silver-Chalcogenolate Cluster-Based Metal-Organic Framework. *Nat. Chem.* **2017**, *9*, 689−697.
(30) Huang, R. W.; Dong, X. Y.; Yan, B. J.; Du, X. S.; Wei, D. H.; Zang, S. Q.; Mak, T. C. W. Tandem Silver Cluster Isomerism and Mixed Linkers to Modulate the Photoluminescence of Cluster-Assembled Materials. *Angew. Chem., Int. Ed.* **2018**, *57*, 8560−8566.
(31) Dong, X.-Y.; Huang, H.-L.; Wang, J.-Y.; Li, H.-Y.; Zang, S.-Q. A Flexible Fluorescent SCC-MOF for Switchable Molecule Identification and Temperature Display. *Chem. Mater.* **2018**, *30*, 2160−2167.
(32) Alhilaly, M. J.; Huang, R.-W.; Naphade, R.; Alamer, B.; Hedhili, M. N.; Emwas, A.-H.; Maity, P.; Yin, J.; Shkurenko, A.; Mohammed, O. F.; Eddaoudi, M.; Bakr, O. M. Assembly of Atomically Precise Silver Nanoclusters into Nanocluster-Based Frameworks. *J. Am. Chem. Soc.* **2019**, *141*, 9585−9592.
(33) Dong, X. Y.; Si, Y.; Yang, J. S.; Zhang, C.; Han, Z.; Luo, P.; Wang, Z. Y.; Zang, S. Q.; Mak, T. C. W. Ligand Engineering to Achieve Enhanced Ratiometric Oxygen Sensing in a Silver Cluster-Based Metal-Organic Framework. *Nat. Commun.* **2020**, *11*, 3678−3679.
(34) Wu, X.-H.; Luo, P.; Wei, Z.; Li, Y.-Y.; Huang, R.-W.; Dong, X.-Y.; Li, K.; Zang, S.-Q.; Tang, B. Z. Guest-Triggered Aggregation-Induced Emission in Silver Chalcogenolate Cluster Metal-Organic Frameworks. *Adv. Sci.* **2019**, *6*, 1801304.
(35) Wei, Z.; Wu, X. H.; Luo, P.; Wang, J. Y.; Li, K.; Zang, S. Q. Matrix Coordination Induced Emission in a Three-Dimensional Silver Cluster-Assembled Material. *Chem.—Eur. J.* **2019**, *25*, 2750−2756.
(36) Wu, X.-H.; Wei, Z.; Yan, B.-J.; Huang, R.-W.; Liu, Y.-Y.; Li, K.; Zang, S.-Q.; Mak, T. C. W. Mesoporous Crystalline Silver-Chalcogenolate Cluster-Assembled Material with Tailored Photoluminescence Properties. *CCS Chem.* **2019**, *1*, 553−560.
(37) Zhao, M.; Huang, S.; Fu, Q.; Li, W.; Guo, R.; Yao, Q.; Wang, F.; Cui, P.; Tung, C. H.; Sun, D. Ambient Chemical Fixation of CO_2 Using a Robust Ag_{27} Cluster-Based Two-Dimensional Metal-Organic Framework. *Angew. Chem.* **2020**, *132*, 20206−20211.
(38) Cao, M.; Pang, R.; Wang, Q.-Y.; Han, Z.; Wang, Z.-Y.; Dong, X.-Y.; Li, S.-F.; Zang, S.-Q.; Mak, T. C. W. Porphyrinic Silver Cluster Assembled Material for Simultaneous Capture and Photocatalysis of Mustard-Gas Simulant. *J. Am. Chem. Soc.* **2019**, *141*, 14505−14509.
(39) Xu, M.; Liang, T.; Shi, M.; Chen, H. Graphene-Like Two-Dimensional Materials. *Chem. Rev.* **2013**, *113*, 3766−3798.
(40) Banerjee, D.; Hu, Z.; Pramanik, S.; Zhang, X.; Wang, H.; Li, J. Vapor phase detection of nitroaromatic and nitroaliphatic explosives by fluorescence active metal−organic frameworks. *CrystEngComm* **2013**, *15*, 9745−9750.
(41) Jurcic, M.; Peveler, W. J.; Savory, C. N.; Scanlon, D. O.; Kenyon, A. J.; Parkin, I. P. The Vapour Phase Detection of Explosive Markers and Derivatives Using Two Fluorescent Metal-Organic Frameworks. *J. Mater. Chem. A* **2015**, *3*, 6351−6359.

https://doi.org/10.1021/acs.chemmater.2c00647
Chem. Mater. 2022, 34, 4703−4711